Pressure-Induced Two-Phase Superconductivity in the Rare-Earth Tritelluride $LaTe_3$

Shuyang Wang(王舒阳)[1], Jing Wang(王晶)[1,2], Chao An(安超)[3], Jiaqi Chen(陈嘉琪)[1], Lili Zhang(张丽丽)[4], Yonghui Zhou(周永惠)[1], Xuliang Chen(陈绪亮)[1*], and Zhaorong Yang(杨昭荣)[1,3*]

[1]*Anhui Provincial Key Laboratory of Low-Energy Quantum Materials and Devices, High Magnetic Field Laboratory, HFIPS, Chinese Academy of Sciences, Hefei 230031, China*
[2]*State Key Laboratory of Surface Physics, and Department of Physics, Fudan University, Shanghai 200438, China*
[3]*Institutes of Physical Science and Information Technology, Anhui University, Hefei 230601, China*
[4]*Shanghai Synchrotron Radiation Facility, Shanghai Advanced Research Institute, Chinese Academy of Sciences, Shanghai 201204, China*

(Received 21 January 2026; accepted manuscript online 18 March 2026)

In the rare-earth tritelluride series (RTe$_3$), light members (R = La–Sm) host a unidirectional charge-density-wave (CDW) order, whereas heavy members (R = Tb–Tm) develop both unidirectional and bidirectional CDW orders. Upon chemical doping, both subsets exhibit superconductivity concomitant with suppression of the CDW order(s). In contrast, although pressure-induced superconductivity has been widely reported in the heavy members, its existence in the light members has remained unclear. Here, we establish a comprehensive pressure–temperature phase diagram of the lightest member, $LaTe_3$, using electrical transport, synchrotron x-ray diffraction, and Raman spectroscopy in diamond anvil cells up to 55.8 GPa, revealing two distinct superconducting phases. The first emerges as the CDW is strongly suppressed and rapidly reaches an optimal $T_C \sim 1.5$ K near the CDW collapse at ∼11 GPa, followed by only a weak decrease of T_C over the broad pressure range of 11–36 GPa. The second appears above ∼31 GPa in conjunction with a *Cmcm*-to-*Pmmm* structural transition, marked by an abrupt increase of T_C from ∼1.4 to ∼2.5 K that then increases gradually up to 52.1 GPa.

DOI: 10.1088/0256-307X/43/4/040715 CSTR: 32039.14.0256-307X.43.4.040715

Charge-density-wave (CDW) order and superconductivity are two ubiquitous collective electronic states in condensed-matter systems, and elucidating their complex interplay remains a central and active theme, in part because of their relevance to high-T_C cuprate superconductors.[1,2] Since both CDW order and superconductivity are intimately tied to electron–phonon coupling and Fermi-surface instabilities, chemical pressure (via substitution or intercalation) and physical pressure (via external compression) are widely used as complementary tuning parameters to interrogate CDW-superconductivity competition and/or cooperation across many material families, as they can directly reshape the electronic structure and/or lattice degrees of freedom. A representative example is the intercalation- and pressure-induced dome-shaped superconducting phases in the prototypical CDW compound $TiSe_2$,[3–8] where results from both tuning routes provide complementary constraints and together enable a deeper understanding of the underlying physics.

Rare-earth tritellurides (RTe$_3$), with their relatively simple electronic structures, constitute a well-known model CDW family for probing CDW states and related physics,[9–13] as well as their connections to other collective electronic phenomena like superconductivity.[14] RTe$_3$ crystallizes in an orthorhombic *Cmcm* structure comprising two pseudo-tetragonal Te layers separated by an RTe slab within the unit cell.[15,16] The corrugated RTe slab is insulating, while the Te bilayer forms a two-dimensional conduction band. Because large portions of the Fermi surface exhibit pronounced nesting that can be connected by an approximately single nesting vector, all members develop CDW order(s). Specifically, the light members (R = La–Sm) host a unidirectional (striped) CDW with a much higher transition temperature ($T_{CDW} > 450$ K), whereas the heavy members (R = Tb–Tm) exhibit a unidirectional CDW with $T_{CDW} \sim 240$–380 K and an additional bidirectional (checkerboard) CDW at a lower temperature.[17–22] Upon chemical doping, superconductivity can be induced in both light and heavy members of RTe$_3$ along with suppression of the CDW order(s).[23–25] Under physical pressure, however, the situation is less settled. For heavy members, pressure-induced superconductivity has been widely reported.[26,27] In contrast, progress in exploring high-pressure superconductivity in the light members has been limited, with $CeTe_3$ remaining the primary case study; even there, the results are controversial,[28,29] leaving the existence of pressure-induced superconductivity in the light subset an open question. Notably, under chemical doping, the maximum T_C values in light members (with only a unidirectional CDW) are typically <0.6 K, substantially lower than those in heavy members (hosting both unidirectional and bidirectional CDWs), which reach ∼2.5–3 K.[23] In this context, exploring possible

*Corresponding authors. Email: xlchen@hmfl.ac.cn; zryang@issp.ac.cn
© 2026 Chinese Physical Society and IOP Publishing Ltd. All rights, including for text and data mining, AI training, and similar technologies, are reserved.

high-pressure superconductivity in light members may provide insight into the apparent dichotomy in T_C between the two subsets under doping.

In this Letter, we present a comprehensive high-pressure study of the lightest member, $LaTe_3$, whose lattice structure is shown in Fig. 1(a). $LaTe_3$ hosts the most robust CDW phase in the RTe_3 family, with T_{CDW} exceeding 600 K.[13] We employ a multi-technique approach combining electrical transport, synchrotron x-ray diffraction (XRD), and Raman spectroscopy in diamond-anvil cells (DACs) up to 55.8 GPa. We identify two superconducting phases: the first emerges concomitant with the marked suppression of the CDW order, and the second appears at much higher pressure, accompanied by a structural transition. Implications of these results for the interplay between CDW order(s) and superconductivity are discussed.

Figure 1(b) shows the single-crystal XRD pattern of $LaTe_3$. Only the $(0l0)$ reflections are observed, indicating that the exposed crystal surface is normal to the b axis. The energy-dispersive X-ray spectroscopy (EDXS) analysis in Fig. 1(c) yields an atomic ratio of La:Te = 1:2.96, close to the ideal stoichiometry. The ac-plane resistivity $\rho(T)$ exhibits simple metallic behavior over the entire measured range from 2 to 300 K and the residual-resistivity ratio $RRR = \rho(300\,\mathrm{K})/\rho(2\,\mathrm{K}) = 260$, in accordance with the previous report.[30] These characterizations confirm the high quality of our samples.

Figure 2 shows the temperature dependence of the ac-plane resistance $R(T)$ of single-crystal $LaTe_3$ under pressures up to 52.1 GPa. Starting at 4.0 GPa, the sample retains the metallic behavior observed at ambient pressure.

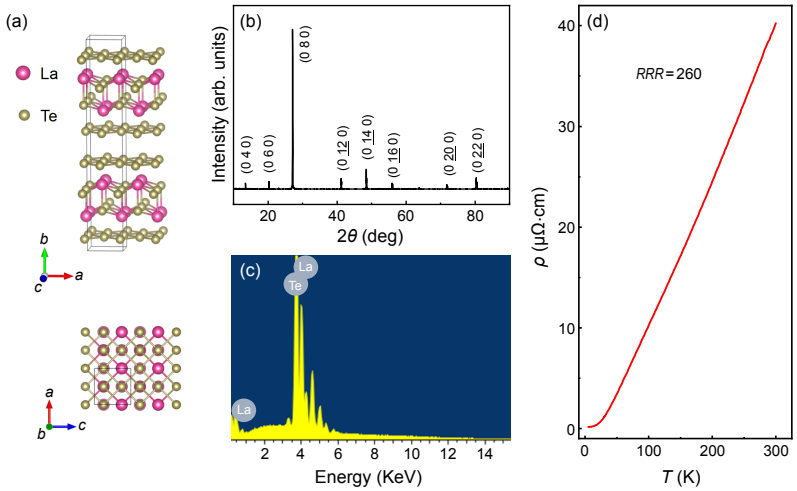

Fig. 1. Basic sample characterization. (a) Crystal structure of $LaTe_3$. (b) Single-crystal XRD pattern of $LaTe_3$. (c) EDXS of $LaTe_3$. (d) Temperature dependence of ac-plane resistivity $\rho(T)$ at ambient pressure.

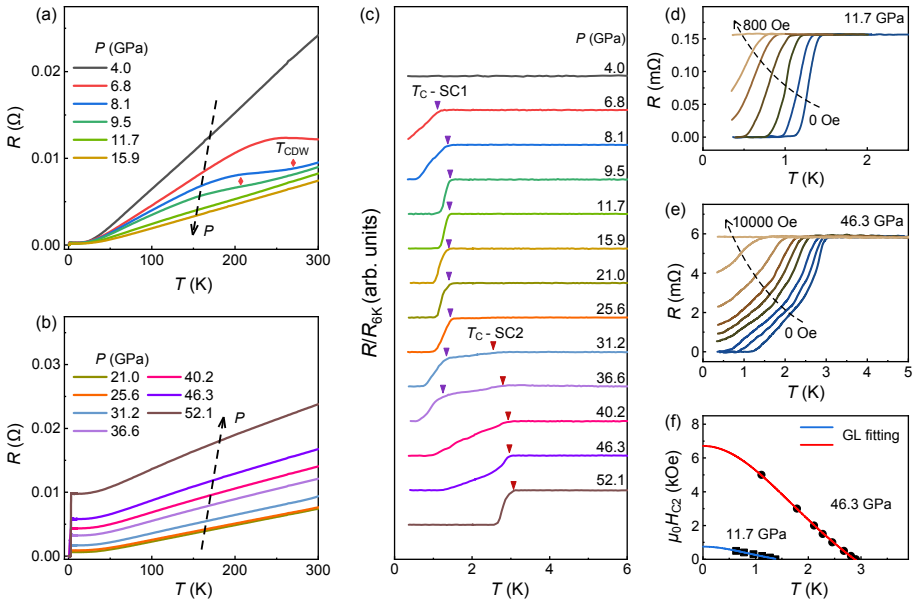

Fig. 2. Evidence for pressure-induced superconductivity in $LaTe_3$. (a) and (b) Temperature dependence of the resistance $R(T)$ under pressures of 4.0–15.9 GPa and 21.0–52.1 GPa, respectively. Rhombuses denote the CDW transition temperature T_{CDW}. (c) Expanded view of the low-temperature $R(T)$ curves; triangles mark the superconducting transition temperature T_C. SC1 and SC2 denote the two pressure-induced superconducting phases. Curves are offset for clarity. (d) and (e) $R(T)$ measured under magnetic fields at 11.7 and 46.3 GPa, respectively. (f) Upper critical field $\mu_0 H_{C2}$ versus T; solid lines are fits to the GL form.

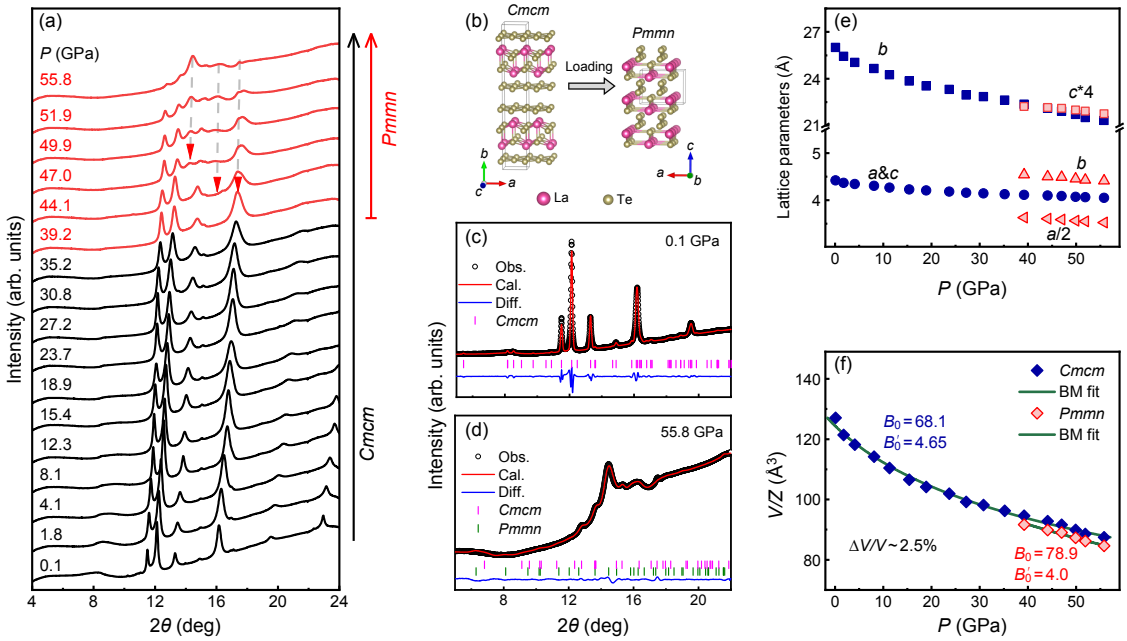

Fig. 3. Pressure evolution of the crystal symmetry in $LaTe_3$. (a) Synchrotron X-ray diffraction patterns of $LaTe_3$ with pressures up to 55.4 GPa ($\lambda = 0.6199$ Å). New reflections emerge above ~39.2 GPa (marked by arrows), evidencing a pressure-induced structural transition. (b) Crystal structures of the low- and high-pressure phases of $LaTe_3$. (c) and (d) Representative Le Bail fits at 0.1 and 55.8 GPa. (e) Lattice parameters as a function of pressure. (f) Volume per formula V/Z versus P. The solid lines are fits to the third-order Birch–Murnaghan EOS.

Upon increasing pressure to 6.8 GPa, a broad hump-like anomaly appears in $R(T)$, which we attribute to partial gap opening associated with the CDW transition, as commonly observed in the RTe_3 family.[31,32] By 8.1 GPa, the CDW transition temperature T_{CDW} is suppressed below 300 K; here, T_{CDW} is defined as the onset temperature of the resistance anomaly. Upon further compression, T_{CDW} shifts to lower temperatures and the amplitude of the hump diminishes progressively; above 11.7 GPa, the hump becomes indiscernible, indicating the gradual suppression and eventual disappearance of long-range CDW order.

Accompanied by the suppression of the CDW, a low-temperature resistance drop emerges, with an onset $T_C \sim 1.1$ K at 0.9 GPa, and a zero-resistance state appears at 8.1 GPa [Fig. 2(c)], indicating the pressure-induced emergence of superconductivity (SC1) in $LaTe_3$. The T_C of SC1 rises rapidly to a maximum of ~1.5 K at 9.5 GPa and then decreases very slightly with further compression up to 30 GPa. At 31.2 GPa, unexpectedly, an additional resistance drop appears at ~2.5 K, indicating the emergence of a second superconducting phase (SC2). Upon further compression, the T_C of SC2 shifts to higher temperatures and the transition width becomes progressively sharper. Both superconducting phases are further corroborated by resistance measurements under magnetic fields at 11.7 and 46.3 GPa [Figs. 2(d) and 2(f)], where the transitions shift to lower temperatures with increasing field. From the extracted $\mu_0 H_{C2}$ data, the upper critical field $\mu_0 H_{C2}$ at the zero-temperature limit is estimated to be 760 Oe (SC1) and 6720 Oe (SC2), according to the Ginzburg–Landau (GL) fits [Fig. 2(f)].

We next performed high-pressure synchrotron XRD to examine possible structural changes associated with the emergence of superconductivity (Fig. 3). The diffraction pattern at 0.5 GPa is well indexed by the ambient-pressure orthorhombic $Cmcm$ structure [Fig. 3(c)]. Upon further compression, no qualitative changes are observed up to 39.2 GPa, aside from the expected gradual shift of Bragg peaks to higher angles due to lattice contraction. Above 39.2 GPa, however, several additional reflections appear [see arrows in Fig. 3(a)], signaling the onset of a pressure-induced structural transition. Notably, reflections from the $Cmcm$ phase persist up to 55.8 GPa, indicating an extended coexistence regime, likely due to a sizable kinetic barrier for this first-order transition. By referencing a previous report in $CeTe_3$ showing a $Cmcm \rightarrow Pmmn$ structural transition near ~36 GPa,[29] we assign the new high-pressure phase of $LaTe_3$ to the same $Pmmn$ structure. The corresponding crystal structures and extracted lattice parameters are summarized in Fig. 3(b). Consistent with this assignment, the XRD patterns are well reproduced by a two-phase model combining the ambient $Cmcm$ and high-pressure $Pmmn$ structures, as shown at 55.8 GPa in Fig. 3(d). The larger ionic size of La compared with Ce likely shifts the transition to higher pressure, consistent with the observed onset near ~40 GPa.

We further extracted the lattice parameters and the equation of state (EOS), as shown in Figs. 5(e) and 5(f). Because the a and c lattice parameters of the $Cmcm$ phase are nearly indistinguishable in our powder XRD data ($a \approx 0.995c$), we constrained the refinement by fixing $a = c$. The EOS was fitted using the third-order Birch–Murnaghan relation,

$$P = \frac{3}{2} B_0 \left[\left(\frac{V_0}{V}\right)^{\frac{7}{3}} - \left(\frac{V_0}{V}\right)^{\frac{5}{3}} \right] \cdot \left\{ 1 + \frac{3}{4}(B_0' - 4) \left[\left(\frac{V_0}{V}\right)^{\frac{2}{3}} - 1 \right] \right\}, \quad (1)$$

where V_0, B_0, and B_0' are the zero-pressure unit-cell volume per formula unit, the bulk modulus, and its first pressure derivative, respectively. The fits yield $B_0 = 68.2(2)$ GPa and $B_0' = 4.65(3)$ for the low-pressure $Cmcm$ phase, and $B_0 = 78.9(2)$ GPa and $B_0' = 4.0(1)$ for the high-pressure $Pmmn$ phase. The volume collapse across the transition is estimated to be ∼2.5%, consistent with a first-order structural transition.

As a sensitive probe of low-energy excitations, Raman spectroscopy has been widely used to investigate CDW states. Figure 4 shows room-temperature Raman spectra of $LaTe_3$ under various pressures. At 0.8 GPa [Fig. 4(a)], the peaks labeled C, F, H, and I are assigned to the ordinary Raman-active phonons B_g^1, A_g^1, A_g^2, and A_g^3, respectively.[9,33,34] In addition, the peaks labeled A, B, F, and G are CDW-related zone-folded (ZF) modes, and peak D corresponds to the CDW amplitude mode (also called Higgs mode).[9] With increasing pressure, modes A and C, and all modes above 80 cm^{-1} exhibit a systematic blueshift due to lattice contraction [Fig. 4(b)]. In contrast, the CDW-related ZF mode B and amplitude mode D display a pronounced anticrossing behavior, similar to that reported in Raman studies of other CDW RTe_3 compounds.[35] At low pressure, the higher-frequency branch (at 74.7 cm^{-1}) has an amplitude character, whereas the lower-frequency branch (at 62.1 cm^{-1}) is phononic. With increasing pressure, the higher branch softens and approaches the lower branch. Near 5.2 GPa, the two branches acquire comparable intensities and repel each other: the amplitude mode is pushed to lower frequency, while the ZF mode shifts upward, leading to an exchange of their dominant character at higher pressure. Such anticrossing is expected only for modes of the same symmetry, whereas modes of different symmetry can cross.[36] Consistent with this, modes B and D share the same (twofold) symmetry, that is A_g mode, giving rise to the pressure-induced anticrossing, whereas the B_g-symmetry phonon mode C crosses the amplitude mode.

The amplitude mode serves as a fingerprint of CDW order: it can be viewed as a soft phonon at the CDW wave vector, coupled to the electronic density modulation and renormalized by amplitude fluctuations of the CDW order parameter. Upon compression, the evolution of this mode is characteristic of pressure-driven CDW suppression: it gradually loses intensity, broadens, and softens toward zero frequency. Such behavior reflects the weakening of the periodic lattice distortion, a progressive flattening of the amplitude-mode potential, and the closure of the CDW gap as the system approaches the CDW phase transition.[37] Finally, both the CDW-related amplitude mode and the ZF mode progressively weaken and become unobservable as the pressure approaches 8 GPa from below, indicating the suppression of CDW order and a transition to a non-CDW phase.

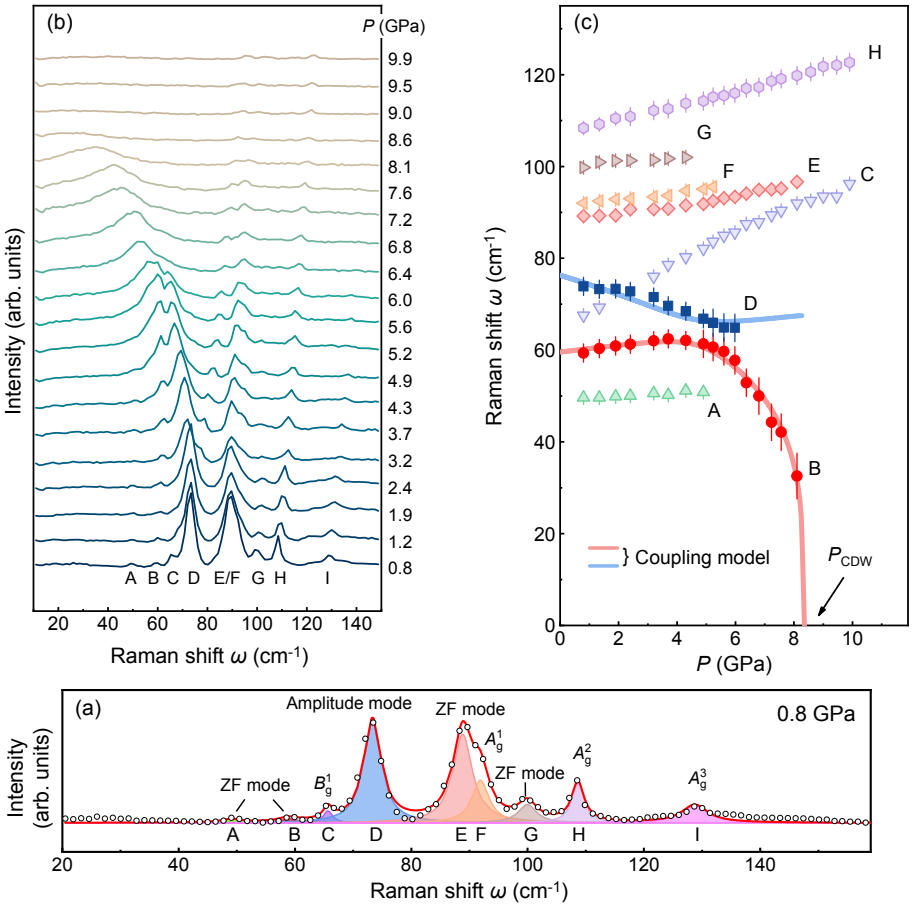

Fig. 4. Pressure-dependent Raman response of $LaTe_3$. (a) Raman spectrum of $LaTe_3$ at 0.8 GPa. (b) Pressure dependence of the Raman spectra at various pressures. (c) Raman-mode frequencies as a function of pressure. Solid lines are coupled-mode fits to the B and D modes, capturing their anticrossing.

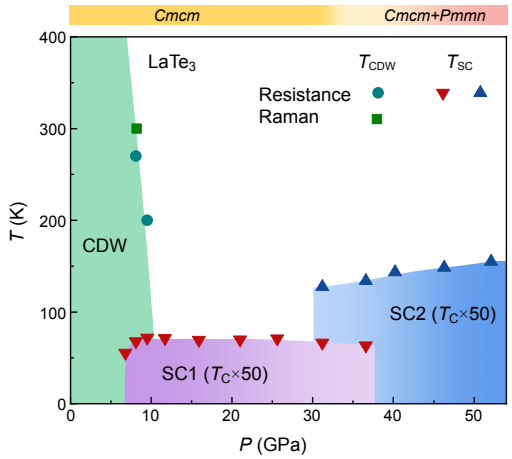

Fig. 5. Temperature–pressure phase diagram of $LaTe_3$. SC1 and SC2 denote the two superconducting phases of $LaTe_3$ under pressure.

The pressure dependences of the Raman-mode frequencies are summarized in Fig. 4(c), obtained by fitting the peaks with Lorentzian line shapes. We now focus on the two modes that exhibit anticrossing. The pressure evolution of the bare CDW amplitude mode can be described within a mean-field form,[37]

$$\omega_{\text{amplitude}}(P) = \omega_0\left(1 - \frac{P}{P_{\text{CDW}}}\right)^{\beta}, \tag{2}$$

where $\omega_{\text{amplitude}}$ is the amplitude-mode frequency, ω_0 is its ambient-pressure value, P_{CDW} is the critical pressure for CDW suppression at 300 K, and β is a critical exponent. The amplitude mode couples to the CDW-related ZF mode through a coupling constant δ, which can be captured by a 2×2 coupling matrix

$$\begin{pmatrix} \omega_{\text{amplitude}} & \delta \\ \delta & \omega_{\text{ZF}} \end{pmatrix}.$$

The eigenvalues of this matrix correspond to the vibrational frequencies observed in Raman spectroscopy, yielding the following expressions for the two branches:

$$\omega_+ = \omega_m + (\Delta^2 + \delta^2)^{1/2}, \tag{3}$$

and

$$\omega_- = \omega_m - (\Delta^2 + \delta^2)^{1/2}, \tag{4}$$

where $\omega_m = (\omega_{\text{amplitude}} + \omega_{\text{ZF}})/2$ and $\Delta = (\omega_{\text{amplitude}} - \omega_{\text{ZF}})/2$. Fitting the coupled-mode model yields $P_{\text{CDW}} = 8.2$ GPa, $\beta = 0.24$, and $\delta = 6.9\,\text{cm}^{-1}$. This critical pressure at 300 K is in excellent agreement with that inferred from transport (see Fig. 5).

Based on the high-pressure results above, we construct the temperature–pressure phase diagram of $LaTe_3$ (Fig. 5), which summarizes the evolution of structure, CDW order, and superconductivity with pressure. As the CDW is strongly suppressed, superconductivity (SC1) emerges and T_{C} increases rapidly. Near ∼11 GPa, T_{C} reaches a maximum as the CDW collapses completely, followed by a pressure-inert T_{C} over a broad pressure range of 11–40 GPa. This evolution cannot be captured in a straightforward manner by the classic Bardeen–Cooper–Schrieffer framework, in which CDW order and superconductivity simply compete for the same portions of the Fermi surface.[38,39] Similar behavior has also been reported in pressurized 2H-TaS_2[40] and 2H-$NbSe_2$,[41] where the microscopic mechanism of pressure-inert T_{C} likewise remains unresolved.

It is instructive to compare our results with prior data across the RTe_3 family and other prototypical CDW materials. As discussed above, chemical doping (e.g., Pd intercalation) suppresses the CDW and induces superconductivity in RTe_3, yet the resulting maximum T_{C} values differ markedly between light and heavy members, i.e., typically <0.6 K for the former and 2–3 K for the latter.[23] In contrast, in our pressure study of $LaTe_3$, the maximum $T_{\text{C}} \sim 1.5$ K is comparable to that reported for heavy RTe_3 under pressure.[27] Compared with the relatively "clean" tuning provided by physical pressure, Pd intercalation is generally accompanied by appreciable disorder and local strain. Indeed, Pd intercalation has been shown to frustrate long-range CDW order and to pin short-range CDW correlations.[25] Such disorder may couple distinctly to the underlying CDW landscape: in light members with a single CDW order, it may predominantly suppress superconductivity by enhancing quasiparticle scattering, whereas in heavy members with multiple competing CDW orders, disorder could instead promote superconductivity by enhancing fluctuations. From this perspective, spatial inhomogeneity of the CDW order may play an important role in enhancing superconductivity in RTe_3, reminiscent of scenarios discussed for $HgBa_2CuO_{4+y}$[42] and $TiSe_2$.[5–8] This possibility may in turn suggest that $LaTe_3$ hosts more than a single CDW instability, consistent with recent reports of additional CDW signatures in this material.[43]

Above 31.2 GPa, a second superconducting state (SC2) with a higher transition temperature emerges. Around the same critical pressure, $LaTe_3$ undergoes a structural transition from *Cmcm* to *Pmmn*, indicating that SC2 is associated with the high-pressure *Pmmn* phase. A plausible scenario is that the enhancement of T_{C} is driven by increased three-dimensionality as the structure evolves from quasi-two-dimensional layering toward a more three-dimensional framework, enabled by Te–Te bonding between adjacent van der Waals layers. A similar enhancement of T_{C}, accompanied by a pressure-induced dimensional crossover via interlayer S–S bonding and associated multiband effects, has been reported in 1T-TaS_2.[44] The high-pressure *Pmmn* phase coexists with the pristine *Cmcm* phase over a wide pressure range, consistent with the SC2 transition broadening over an extended pressure interval.

In summary, we have investigated the pressure-dependent electrical transport and structural evolution of the CDW material $LaTe_3$ and observe two pressure-induced superconducting transitions. Suppression of the CDW order gives rise to the first superconducting phase (SC1), whereas a pressure-driven structural transition triggers the emergence of a second phase (SC2). These results fill a key gap in understanding high-pressure superconductivity in the light RTe_3 members and, complementary to chemical doping, provide new insight into the interplay between CDW order(s) and superconductivity across this materials family.

Methods.

Sample Preparation. Single crystals of $LaTe_3$ were grown by a flux method using alkali-metal chlorides. Stoichiometric amounts of La ingot and Te powder (total mass 0.8 g) were sealed in an evacuated quartz ampoule together with 1.6 g of flux (LiCl:RbCl = 1:1). All sample preparation steps were carried out in an argon-filled glove box. The ampoule was held at 650 ℃ for 2 days, cooled to 540 ℃ over 5 days, and furnace-cooled to room temperature. Shiny $LaTe_3$ single crystals with golden surfaces were mechanically cleaved using Scotch tape and used for subsequent measurements. Single-crystal XRD patterns were collected at room temperature using an in-lab diffractometer with Cu-K_α radiation ($\lambda = 1.54184$ Å). The elemental composition was characterized by EDXS.

High-Pressure Measurements. High-pressure resistance measurements were performed in a nonmagnetic Be–Cu DAC using NaCl powder as the pressure-transmitting medium, together with an in-house multifunctional physical-property measurement system with a ^{3}He insert providing a temperature range of 0.4–300 K. The DAC sample-loading procedure for transport followed Ref. [45]. High-pressure angle-dispersive synchrotron XRD experiments were carried out at beamline BL15U1 of the Shanghai Synchrotron Radiation Facility ($\lambda = 0.6199$ Å). Finely ground $LaTe_3$ powders were loaded into a Mao-Bell DAC with Daphne 7373 as the pressure-transmitting medium. High-pressure Raman measurements were performed using a 532-nm laser with Daphne 7373 as the pressure-transmitting medium. The laser power was maintained below 0.5 mW with a spot size of $\sim 5 \times 5\,\mu m^2$ to minimize sample damage and laser-heating effects. For all high-pressure experiments, sample loading was conducted in an argon atmosphere inside a glove box. Pressures were determined at room temperature by the ruby fluorescence method.

Acknowledgements. This work was supported by the National Key R&D Program of China (Grant Nos. 2023YFA1406102, 2022YFA1602603, 2023YFA1608903, and 2024YFA1611101), the National Natural Science Foundation of China (Grant Nos. 12404065, 12374049, and 12174395), the Basic Research Program of the Chinese Academy of Sciences Based on Major Scientific Infrastructures (Grant No. JZHKYPT-2021-08), and the Anhui Provincial Major S&T Project (Grant No. S202305A12020005). Y.H.Z. was supported by the Natural Science Foundation of Anhui Province (Grant No. 2308085MA16). S.Y.W. was supported by the China Postdoctoral Science Foundation (Grant No. 2023M743542), and the Director's Foundation of Hefei Institutes of Physical Science, Chinese Academy of Sciences (Grant No. YZJJ2024QN41). C.A. was supported by the Key Project of Natural Scientific Research of Universities in Anhui Province (Grant No. 2024AH050087). Portions of this work were performed at the ultrahigh pressure physical property measurement system (UP3MS, 31125.02.SHMFF.WM5) of Steady High Magnetic Field Facility (SHMFF, 31125.02.SHMFF), Chinese Academy of Sciences. The synchrotron XRD measurements were done at hard X-ray micro-focusing beamline BL15U1 (31124.02.SSRF.BL15U1) of the Shanghai Synchrotron Radiation Facility.

References

[1] da Silva Neto E H, Aynajian P, Frano A, Comin R, Schierle E, Weschke E, Gyenis A, Wen J, Schneeloch J, and Xu Z 2014 *Science* **343** 393
[2] Hayden S M and Tranquada J M 2024 *Annu. Rev. Condens. Matter Phys.* **15** 215
[3] Morosan E, Zandbergen H W, Dennis B, Bos J, Onose Y, Klimczuk T, Ramirez A, Ong N, and Cava R J 2006 *Nat. Phys.* **2** 544
[4] Kusmartseva A F, Sipos B, Berger H, Forro L, and Tutiš E 2009 *Phys. Rev. Lett.* **103** 236401
[5] Joe Y I, Chen X M, Ghaemi P, Finkelstein K D, de La Peña G A, Gan Y, Lee J C T, Yuan S, Geck J, MacDougall G J, Chiang T C, Cooper S L, Fradkin E, and Abbamonte P 2014 *Nat. Phys.* **10** 421
[6] Yan S C, Iaia D, Morosan E, Fradkin E, Abbamonte P, and Madhavan V 2017 *Phys. Rev. Lett.* **118** 106405
[7] Kogar A, de la Pena G A, Lee S, Fang Y, Sun S X L, Lioi D B, Karapetrov G, Finkelstein K D, Ruff J P C, Abbamonte P, and Rosenkranz S 2017 *Phys. Rev. Lett.* **118** 027002
[8] Novello A M, Spera M, Scarfato A, Ubaldini A, Giannini E, Bowler D, and Renner C 2017 *Phys. Rev. Lett.* **118** 017002
[9] Wang Y, Petrides I, McNamara G, Hosen M M, Lei S, Wu Y C, Hart J L, Lv H Y, Yan J, and Xiao D 2022 *Nature* **606** 896
[10] Singh B, McNamara G, Kim K M *et al.* 2025 *Nat. Phys.* **21** 1578
[11] Straquadine J, Ikeda M, and Fisher I 2022 *Phys. Rev. X* **12** 021046
[12] Sarkar S, Bhattacharya J, Sadhukhan P, Curcio D, Dutt R, Singh V K, Bianchi M, Pariari A, Roy S, Mandal P and 2023 *Nat. Commun.* **14** 3628
[13] Kogar A, Zong A, Dolgirev P E, Shen X, Straquadine J, Bie Y-Q, Wang X, Rohwer T, Tung I, and Yang Y 2020 *Nat. Phys.* **16** 159
[14] Yumigeta K, Qin Y, Li H, Blei M, Attarde Y, Kopas C, and Tongay S 2021 *Adv. Sci.* **8** 2004762
[15] Kang J S, Seong S, Lee E, Kwon Y S, Kim K, Kim J, Kim H, and Min B 2024 *Phys. Rev. Mater.* **8** 080301
[16] Brouet V, Yang W, Zhou X, Hussain Z, Moore R, He R, Lu D, Shen Z, Laverock J, and Dugdale S 2008 *Phys. Rev. B* **77** 235104
[17] Malliakas C D and Kanatzidis M G 2006 *J. Am. Chem. Soc.* **128** 12612
[18] DiMasi E, Aronson M, Mansfield J, Foran B, and Lee S 1995 *Phys. Rev. B* **52** 14516
[19] Banerjee A, Feng Y, Silevitch D, Wang J, Lang J, Kuo H H, Fisher I, and Rosenbaum T 2013 *Phys. Rev. B* **87** 155131
[20] Brouet V, Yang W L, Zhou X J, Hussain Z, Moore R G, He R, Lu D H, Shen Z X, Laverock J, Dugdale S B, Ru N, and Fisher I R 2008 *Phys. Rev. B* **77** 235104
[21] Sacchetti A, Degiorgi L, Giamarchi T, Ru N, and Fisher I R 2006 *Phys. Rev. B* **74** 125115
[22] Hu B, Cheng B, Yuan R, Dong T, and Wang N 2014 *Phys. Rev. B* **90** 085105
[23] He J B, Wang P P, Yang H X, Long Y J, Zhao L X, Ma C, Yang M, Wang D M, Shangguan X C, Xue M Q, Zhang P, Ren Z A, Li J Q, Liu W M, and Chen G F 2016 *Supercond. Sci. Tech.* **29** 065018
[24] Lou R, Cai Y, Liu Z, Qian T, Zhao L, Li Y, Liu K, Han Z, Zhang D, and He J 2016 *Phys. Rev. B* **93** 115133
[25] Straquadine J A W, Weber F, Rosenkranz S, Said A H, and Fisher I R 2019 *Phys. Rev. B* **99** 235138
[26] Hamlin J J, Zocco D A, Sayles T A, Maple M B, Chu J H, and Fisher I R 2009 *Phys. Rev. Lett.* **102** 177002

[27] Zocco D, Hamlin J, Grube K, Chu J H, Kuo H H, Fisher I, and Maple M 2015 *Phys. Rev. B* **91** 205114
[28] Zocco D A, Hamlin J J, Sayles T A, Maple M B, Chu J H, and Fisher I R 2009 *Phys. Rev. B* **79** 134428
[29] Li J, Feng J, Wang D, Peng S, Li M, Wang H, Xu Y, Zhao T, Zhao B, and Jiang S 2024 *Phys. Rev. B* **109** 094119
[30] Pariari A, Koley S, Roy S, Singha R, Laad M S, Taraphder A, and Mandal P 2021 *Phys. Rev. B* **104** 155147
[31] Ru N, Condron C, Margulis G, Shin K, Laverock J, Dugdale S, Toney M, and Fisher I 2008 *Phys. Rev. B* **77** 035114
[32] Sinchenko A A, Grigoriev P D, Lejay P, and Monceau P 2014 *Phys. Rev. Lett.* **112** 036601
[33] Lazarević N, Popović Z, Hu R, and Petrovic C 2011 *Phys. Rev. B* **83** 024302
[34] Chen Y N, Wang P P, Wu M H, Ma J L, Wen S H, Wu X F, Li G M, Zhao Y, Wang K D, and Zhang L Y 2019 *Appl. Phys. Lett.* **115** 151905
[35] Kopaczek J, Li H, Yumigeta K, Sailus R, Sayyad M Y, Moosavy S T R, Kudrawiec R, and Tongay S 2022 *J. Mater. Chem. C* **10** 11995
[36] Lucazeau G 2003 *J. Raman Spectrosc.* **34** 478
[37] Grüner G 1988 *Rev. Mod. Phys.* **60** 1129
[38] Gabovich A, Voitenko A, and Ausloos M 2002 *Phys. Rep.* **367** 583
[39] Chen C W, Choe J, and Morosan E 2016 *Rep. Prog. Phys.* **79** 084505
[40] Zhao X M, Zhang K, Cao Z Y, Zhao Z W, Struzhkin V V, Goncharov A F, Wang H K, Gavriliuk A G, Mao H K, and Chen X J 2020 *Phys. Rev. B* **101** 134506
[41] Moulding O, Osmond I, Flicker F, Muramatsu T, and Friedemann S 2020 *Phys. Rev. Res.* **2** 043392
[42] Campi G, Bianconi A, Poccia N, Bianconi G, Barba L, Arrighetti G, Innocenti D, Karpinski J, Zhigadlo N D, Kazakov S M, Burghammer M, Zimmermann M, Sprung M, and Ricci A 2015 *Nature* **525** 359
[43] Xian G Y, Jiang P J, Li Y H, Shi X W, Han G Y, Yang H T, Zhang Y Y, Lin X, and Gao H J 2023 *Chin. Phys. Lett.* **40** 087402
[44] Dong Q, Li Q, Li S, Shi X, Niu S, Liu S, Liu R, Liu B, Luo X, and Si J 2021 *npj Quantum Mater.* **6** 20
[45] Wang S Y, Chen X L, An C, Zhou Y, Zhou Y H, Gu C C, Zhang L L, Yang X P, and Yang Z R 2021 *Phys. Rev. B* **103** 134518